ACS APPLIED MATERIALS & INTERFACES

Research Article

www.acsami.org

Structural Evolution and the Control of Defects in Atomic Layer Deposited $HfO_2-Al_2O_3$ Stacked Films on GaAs

Yu-Seon Kang,[†] Dae-Kyoung Kim,[†] Kwang-Sik Jeong,[†] Mann-Ho Cho,[†,*] Chung Yi Kim,[†,‡] Kwun-Bum Chung,[§] Hyoungsub Kim,[⊥] and Dong-Chan Kim[#]

[†]Institute of Physics and Applied Physics, Yonsei University, Seoul, 120-749, Korea

[§]Department of Physics, Dankook University, Cheonan, 330-714, Korea

[⊥]School of Materials Science and Engineering, Sungkyunkwan University, Suwon 440-746, Korea

[#]Process Development Team, Semiconductor R&D Center, Samsung Electronics Co., Ltd., Yongin 446-711, Korea

ABSTRACT: The structural characteristics and interfacial reactions of bilayered dielectric stacks of 3 nm HfO_2/2 nm Al_2O_3 and 3 nm Al_2O_3/2 nm HfO_2 on GaAs, prepared by atomic layer deposition (ALD), were examined during film growth and the postannealing process. During the postdeposition annealing (PDA) of the Al_2O_3/HfO_2/GaAs structures at 700 °C, large amounts of Ga oxides were generated between the Al_2O_3 and HfO_2 films as the result of interfacial reactions between interdiffused oxygen impurities and out-diffused atomic Ga. However, in the case of the HfO_2/Al_2O_3/GaAs structures, the presence of an Al_2O_3 buffer layer effectively blocked the out-diffusion of atomic Ga, thus suppressing the formation of Ga oxide. Microstructural analyses showed that HfO_2 films that were deposited on Al_2O_3/GaAs had completely crystallized during the PDA process, even at 700 °C, because of the Al_2O_3 diffusion barrier. Capacitance−voltage measurements showed a relatively large frequency dispersion of the Al_2O_3/HfO_2/GaAs structure in accumulation capacitance compared to the HfO_2/Al_2O_3/GaAs structure due to a higher interface state density. Conductance results revealed that the Al_2O_3 buffer layer on GaAs resulted in a significant reduction in gap states in GaAs. The induced gap state in the Al_2O_3/HfO_2/GaAs structure originated from the out-diffusion of atomic Ga into the HfO_2 film. Density functional theory calculations supported this conclusion.

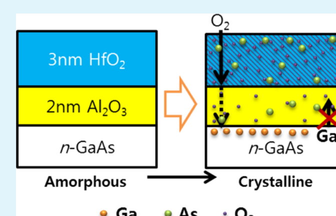

KEYWORDS: *HfO_2, GaAs, Al_2O_3 passivation, Ga diffusion, interstitial Ga, interfacial reaction*

1. INTRODUCTION

As the dimensions of SiO_2/Si-based complementary metal oxide semiconductor (MOS) devices decrease, physical and electrical problems such as poor reliability, frequency dispersion, and high leakage currents increase. To overcome this degradation in performance, researchesr are considering advanced gate stacked MOS structures based on high-κ oxides and III−V compound semiconductors for use in future MOS device applications. Among the many promising candidates for high-κ/III−V structures, HfO_2/GaAs and Al_2O_3/GaAs have electrical properties that are acceptable for use in MOS devices.[1−4] The use of atomic layer deposition (ALD) to achieve high-κ oxide growth (HfO_2 and Al_2O_3) on GaAs results in a high-quality interface without Ga and As oxidation states through a self-cleaning effect.[5,6] However, Ga−O and As−O bonding states are readily formed in HfO_2/GaAs devices after a postannealing treatment.[7,8] The formation of interfacial Ga and As can result in defective states in the electronic structures of high-κ oxides, which can reduce electrical performance.[9−11] The $Al_2O_3/HfO_2/Al_2O_3$/GaAs structure has been proposed to have a promising electrical performance because of the formation of a thermally stable interface.[8] To inhibit the formation of Ga and As oxides, process optimization in the stack structure is essential for developing advanced MOS applications. Therefore, comprehensive physical, electrical, and theoretical analyses of the interfacial states in stacked dielectrics films on GaAs are needed, if the interfacial reaction process for advanced MOS applications is to be completely understood.

In this study, we investigated the physical and electrical properties of bilayer, stacked, high-κ oxide films grown by atomic layer deposition (ALD) on GaAs, consisting of HfO_2 (3 nm)/Al_2O_3 (2 nm)/GaAs and Al_2O_3 (3 nm)/HfO_2 (2 nm)/GaAs structures. We focused on the control of defect states by investigating interfacial reactions in two samples in which the stacking sequences of the Al_2O_3 layer in a $HfO_2-Al_2O_3$ stacked film system were different. X-ray photoelectron spectroscopy (XPS) data indicated that the reduction in native oxide content on GaAs was dependent on the stack structure; specifically, a nearly clean interface between high-κ oxide/GaAs substrate was found for Al_2O_3/HfO_2/GaAs but was not observed for HfO_2/Al_2O_3/GaAs. Large amounts of Ga−O states in Al_2O_3/HfO_2/GaAs were generated during annealing at a temperature of 700 °C, compared with the HfO_2/Al_2O_3/GaAs structure. Consequently, the HfO_2 film that was deposited on Al_2O_3/GaAs was completely crystallized after postdeposition annealing (PDA) at 700 °C because the Al_2O_3 bottom layer blocked the out-diffused Ga from the GaAs substrate. On the other hand, an amorphous structure was maintained in the HfO_2

Received: November 22, 2012
Accepted: February 25, 2013
Published: February 25, 2013

ACS Publications © 2013 American Chemical Society

bottom layer, which was composed of a mixed structure of out-diffused Ga and HfO_2. Finally, measured (based on DFT results) and calculated defect states (using a conductance method) showed that the gap state in GaAs originated from interstitial Ga in HfO_2 films that was significantly suppressed as the Al_2O_3 layer came into contact with the GaAs substrate.

2. EXPERIMENTAL SECTION

We prepared two alternative high-κ oxide films stacked on a GaAs substrate: (i) Al_2O_3/HfO_2/GaAs (AH/GaAs) and (ii) HfO_2/Al_2O_3/GaAs (HA/GaAs). Before the deposition of high-κ oxide films, the native oxides on Si-doped *n*-type GaAs(100) substrates were removed by wet cleaning using a dilute solution of buffed oxide etchant (BOE, NH_4F:HF = 6:1) to 1% for 2 min. After the BOE treatment, the samples were immediately transferred to the ALD chamber. It took less than 20 s to transfer the sample to the load lock chamber in ALD. HfO_2 and Al_2O_3 films were grown on the BOE-treated GaAs surface using the ALD system with tetrakis (ethylmethylamido) hafnium (TEMAHf) as a Hf metal precursor and trimethyl aluminum (TMA) as an Al metal precursor. H_2O vapor was the oxygen source and N_2 gas was the purge gas for film growth. The substrate temperature was maintained at a uniform 320 °C and a working pressure at 1 Torr was used for the deposition of the high-κ oxide films. For the Al_2O_3/HfO_2/GaAs stack structure, the HfO_2 and Al_2O_3 layers were deposited using 26 cycles and 40 cycles, respectively. For the HfO_2/Al_2O_3/GaAs stack structure, 27 cycles and 39 cycles were used to deposit the Al_2O_3 and HfO_2 layers, respectively. Films were annealed at 700 °C by a PDA process for 1 min in a N_2 environment. Microstructural analyses of the stacked HfO_2−Al_2O_3 films on GaAs involved the use of high-resolution transmission electron microscopy (HRTEM) and X-ray diffraction (XRD). Changes in the energy band gaps in bilayer high-κ oxide films were compared by reflection electron energy loss spectroscopy (REELS) with a primary beam energy of 1.0 keV. The chemical states for the bilayer films grown on GaAs were examined by high resolution X-ray photoelectron spectroscopy (XPS) at the Korea Basic Science Institute in Jeonju, Korea. XPS core-level spectra of Hf 4*f* (Ga 3d), As 3d, Al 2p, and C 1s were obtained using a monochromatic Al $K\alpha$ X-ray source ($h\nu$ = 1486.7 eV) with a pass energy of 20 eV. The GaAs substrates were electrically grounded to the electron analyzer to eliminate charging effects. Binding energies were calibrated by core-level spectra using the C 1*s* spectrum (284.5 eV). To deconvolute the XPS core-level spectra, background was removed by Shirley-type subtraction. Full widths at half-maximum (fwhm) of the constituent peaks were kept constant. Fitting curves were determined by Gaussian and Lorentzian distributions, in which the Gaussian distribution ratio was higher than 80%. In addition, for the case of the Hf 4f, Ga 3d, and As 3d doublets, the intensity ratio of the spin−orbit splitting was determined by the probability of transition to such a state during photoionization. Energy separation for Hf 4f, Ga 3d, and As 3d doublets were fixed at 1.66, 0.45, and 0.69 eV, respectively. Sputtering using Ne gas was applied during the XPS measurement to obtain data concerning chemical states along the depth direction as a function of sputtering time. The take off angle during the measurement was fixed at 20° to the sample surface. A gas pressure of 5 mPa was maintained at each sputtering step, with a sputtering power of 1 kV, and a sputtering time of 0.5 min. In general, As 3d core level spectra are used for XPS analyses because they reflect the most sensitive chemical state of the materials. However, we collected As 2*p* core level spectra for depth profiling because the As 3d spectra overlap with Hf 5p spectra. The mean free path of a photo electron in the As 2p core level is much shorter than that for the As 3d core level because photo electrons in the As 2p core level has a lower kinetic energy (155−165 eV) than photoelectrons in the As 3d core level (1438−1448 eV). Moreover, we used a normal take off angle during the As 3d measurement, while a 20° take off angle was used in the case of the As 2p measurements. The findings indicate that the intensity in the As 3d spectra includes information for all regions of the film, while the intensity in As 2p spectra provides information on the very surface region of the film. For electrical characterization, a metal oxide semiconductor capacitor (MOSCAP) was fabricated by sputtering of a 120 nm thick metal (TiN) top contact with 6.4×10^{-5} cm^2 areas through a shadow mask. Capacitance−voltage (C−V) characteristics and the conductance were measured using an Agilent E4980A LCR meter. The density of the interfacial defect state (D_{it}) was determined by parallel conductance $(G_p/\omega)_{max}$, and the energy level of the defect state was determined from frequency measurements. The G_p/ω value was calculated using the equation below[12]

$$\frac{G_p}{\omega} = \frac{\omega {C_{OX}}^2 G_m}{[{G_m}^2 + \omega^2 (C_{ox} - C_m)^2]}$$

where ω is $2\pi f$, and frequency (f) is measured from 1 kHz to 1 MHz. C_{ox} is the gate oxide capacitance, G_m and C_m are the measured conductance and capacitance. A correction term was considered for the high leakage current caused by the thin film thickness. The D_{it} in depletion is proportional to the peak values of G_p/ω,

$$D_{it} \approx 2.5 \frac{(G_p/\omega)_{max}}{Aq}$$

where A is the area of the electrode and q the elemental charge. The trap energy level is given by Shockley−Read−Hall statistics for the capture and emission rates using the following equation, which describes the relationship between the time constant τ of the trap and the frequency

$$f = \frac{1}{2\pi\tau} = \frac{v_{th}\sigma N}{2\pi} \exp\left[\frac{-\Delta E}{k_B T}\right]$$

where v_{th} is the average thermal velocity of the majority carrier, N is the effective density of states of the majority carrier band, and σ is the captured cross section of the trap state. We evaluated the energy level of the defect states within 0.21 eV-0.35 eV below the conduction band edge for GaAs under the measurement conditions (frequency between 1 kHz and 1000 kHz and temperature at 25 °C). In addition, density functional theory (DFT) calculations were employed to evaluate the energy levels and the energy of formation of the defect states. Calculations were performed using VASP code with the exchange correlation function of the generalized gradient approximation (GGA) PBESol. Geometry optimization for the unit cell of each structure (P21/c HfO_2 and $R\bar{3}c$ Al_2O_3) was performed. The conventional cell for both HfO_2 and Al_2O_3 was calculated using 7 7 7 k-points. To minimize interactions between charged defects, 2 2 2 (HfO_2) and 2 2 2 (Al_2O_3) supercells were used for the defect calculation. Gamma k-points for geometry optimization and $3 \times 3 \times 3$ k-points were used for calculations of the energy state and density of the states. All calculations were carried out using a plane wave cutoff energy of 500 eV.

3. RESULTS AND DISCUSSION

Cross-sectional HRTEM images of as-deposited AH/GaAs and HA/GaAs samples are shown in Figure 1(a). Oxide layer thickness was controlled at ~2.0 nm (±0.3) for the bottom layer and ~3.0 nm (±0.4) for the top layer. For both samples, the HfO_2 and Al_2O_3 films grew well as an amorphous phase. The atomically sharp and uniform interface between the bottom oxides and GaAs are due to the self-cleaning effect at the initial growth stage, with the Ga and As oxides on GaAs being effectively removed during the self-limited ALD process by the TMA and TEMAHf precursors.[5,13] However, distinguishing the interfacial layer from the bottom oxide layers and the substrate was difficult because of the presence of a thin local interfacial oxide layer that was not easily detected using HRTEM. To collect detailed information on the interfacial layer of the bottom oxide/GaAs, the chemical states of the interfacial layers in the two stack structures were examined using XPS. Figure 1(b) shows the XPS core-level spectra of Hf

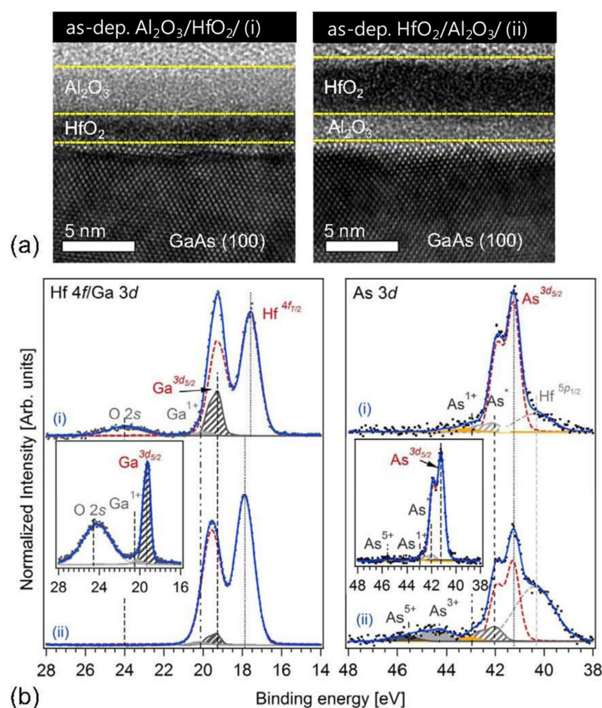

Figure 1. (a) Cross-sectional HR-TEM images of $Al_2O_3/HfO_2/GaAs$ and $HfO_2/Al_2O_3/GaAs$ samples. Similar thicknesses are shown between bilayered stacked high-κ oxide/GaAs samples. (b) XPS Hf 4f/Ga 3d and As 3d core-level spectra for (i) AH/GaAs and (ii) HA/GaAs samples. Inset, Ga 3d and As 3*d* spectra of 4 nm thick single Al_2O_3 film grown on GaAs. High O 2s peak in the Al_2O_3 inset indicates that the O 2*s* peak of AH/GaAs was caused by the relatively thick Al_2O_3 film compared to HA/GaAs.

4f/Ga 3d and the As 3d states for AH/GaAs (upper spectra) and HA/GaAs (bottom spectra) samples. For detailed fitting of the XPS chemical states, the peak position and peak height of the GaAs substrate state that overlapped with the Hf $4f_{5/2}$ state was used as a reference peak for comparisons with other chemical states of Ga and As. Under XPS energy resolution, deconvoluting the chemical states between the Hf 4f and Ga 3d states was performed as follows. The Ga 3*d* states in an as-deposited HA/GaAs sample are comprised of two states of GaAs for the substrate and a Ga^{1+} state for GaO_x.[14] Multiple oxidation states of As^{1+} (AsO_x), As^{3+} (As_2O_3), and As^{5+} (As_2O_5) and the elemental As state (As*) were clearly evident in the As 3d spectra.[14,15] An oxygen 2*s* peak at 24 eV was present in the AH/GaAs sample from the Ga−O, As−O, Hf−O, and Al−O bonding states. In the 3 nm thick HfO_2 film of the Al_2O_3/GaAs sample, an O 2*s* peak was not observed because the intensity of the Hf 4*f* peak was stronger than the O 2*s* peak. The peak ratio of Ga−O (or As−O)/GaAs in Ga 3d (or As 3d) caused by the oxidation states of Ga (or As) indicated that the reaction at the AH/GaAs and HA/GaAs interface occurred. In the AH/GaAs sample, peaks corresponding to As−O bonds were not observed without a peak for As^{1+} at the interface between HfO_2/GaAs. Moreover, the intensity of peaks due to Ga−O bonds were decreased. However, at the HA/GaAs interface, the ratio of the relative peak intensity ratio of the oxidation to the substrate state indicated that large amounts of the Ga^{1+} oxidation state and various As−O bonds had been produced, compared to the AH/GaAs interface. Previous studies reported that differences in the degree of self-cleaning effect can occur when the substrate temperature for optimum ALD reaction conditions for TMA and TEMAHf are not the same.[5,13,15] Specifically, the removal of interfacial oxide is significantly associated with the ligand exchange mechanism, which is critically dependent on the substrate temperature during ALD. Thus, in the HA/GaAs sample, it is possible that the TMA ligands might not react effectively with As−O bonds under a substrate temperature 320 °C during the ALD process. This resulted in a decrease in the self-cleaning effect during the initial growth stage of the ALD-Al_2O_3 on GaAs. The different interfacial oxide states at the interface of the AH/GaAs and HA/GaAs might also be affected by the thickness of the high-*k* dielectric layer, which could reduce oxygen diffusivity. A recent report showed that interfacial oxide regrowth depends on the length of time the sample is exposed to air.[16] For HA/GaAs, oxygen that reacts with the GaAs substrate continuously diffuses into the substrate through the relatively thin Al_2O_3 layer, enhancing the Ga^{1+} states caused by Ga−O bonds (Figure 1b). Comparing the chemical state of the 4 nm-thick Al_2O_3 single layer grown on GaAs with the HA/GaAs structure, as shown in the inset of Figure 1b, the Ga and As oxide were significantly reduced in the Al_2O_3 layer on GaAs because the relatively thick Al_2O_3 layer effectively blocked the interdiffusion of oxygen impurities for reoxidation. This result indicates that interfacial reactions between interdiffused oxygen and GaAs are the main cause of reoxidation.

Panels a and b in Figure 2 show XPS spectral changes for postannealed AH/GaAs (upper) and HA/GaAs (lower)

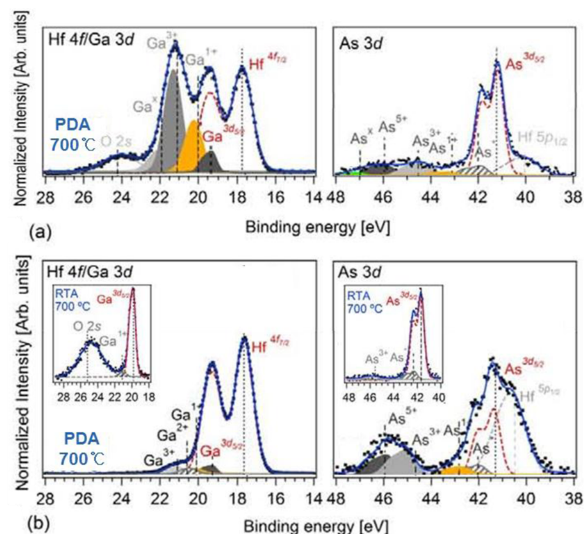

Figure 2. XPS Hf 4f/Ga 3d and Hf 5p/As 3d core-level spectra of annealed (a) $Al_2O_3/HfO_2/GaAs$ and (b) $HfO_2/Al_2O_3/GaAs$ samples. In Hf 4f and Al 2p (not shown) spectra of two samples after PDA at 700 °C, No reaction between metal oxide layers was detected. By Ga 3d, Ga^{1+}, Ga^{2+}, Ga^{3+}, and Ga^x states were associated with GaO_x, GaO, Ga_2O_3, and $Ga(AsO_3)_3$ states, respectively. By As 3d, As^{1+}, As^{3+}, As^{5+}, As*, and As^x states were associated with AsO_x, As_2O_3, As_2O_5, elemental As, and $Ga(AsO_3)_3$ states, respectively. Insets, Ga 3d and As 3d spectra of annealed 4 nm thick single Al_2O_3 films on GaAs at 700 °C.

samples. The two samples were subjected to postannealing treatments in order to examine interfacial reactions and thermal stabilities, which directly influence the electrical performance of high-κ oxide/GaAs devices. As shown in Figure 2, the spectral changes in the Ga 3d and As 3d core-level spectra of two samples after PDA are closely correlated with changes in the

dx.doi.org/10.1021/am302803f | ACS Appl. Mater. Interfaces 2013, 5, 1982−1989

bottom oxide layers that are in contact with GaAs. We compared changes in the chemical bonding ratios of Ga or As oxides using peak areas in the XPS data before and after the annealing treatment (Figure 3). In the case of the AH/GaAs sample, Ga−O bonds were dramatically increased during the PDA at 700 °C, even though the AH/GaAs structure contained a thicker Al_2O_3 layer than the HA/GaAs sample. The reaction mechanism for the high-*k*/GaAs system requires that possible reactants containing oxygen during the reaction process must be taken into consideration. That is, the GaAs substrate can decompose when the temperature of the annealing process exceeds the decomposition temperature, so decomposed atomic Ga and atomic As also likely contribute to the diffusion process as reactants.[17] In the HA/GaAs structure, the diffusion of atomic Ga was suppressed by the Al_2O_3 layer, which acts as a diffusion barrier. This results in the suppression in Ga−O formation during the PDA at 700 °C. An interesting finding was that the changes in As−O states after the PDA at 700 °C were negligible, compared to the changes in Ga−O states. Substantial differences in the behavior of Ga−O and As−O were found, as was also reported in our previous study of HfO_2/GaAs.[6] In the earlier study, we performed medium energy ion-scattering (MEIS) in a HfO_2/GaAs system to investigate the chemical composition of the film in the depth direction. Elemental Ga was observed both at the surface of the HfO_2 film and at the interface between HfO_2/GaAs, while

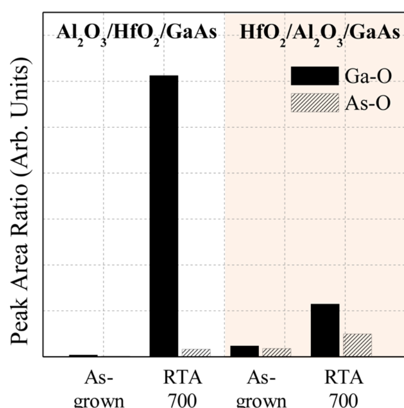

Figure 3. Ga or As oxide ratios using the peak area from XPS data before and after annealing for Al_2O_3/HfO_2/GaAs and HfO_2/Al_2O_3/GaAs samples.

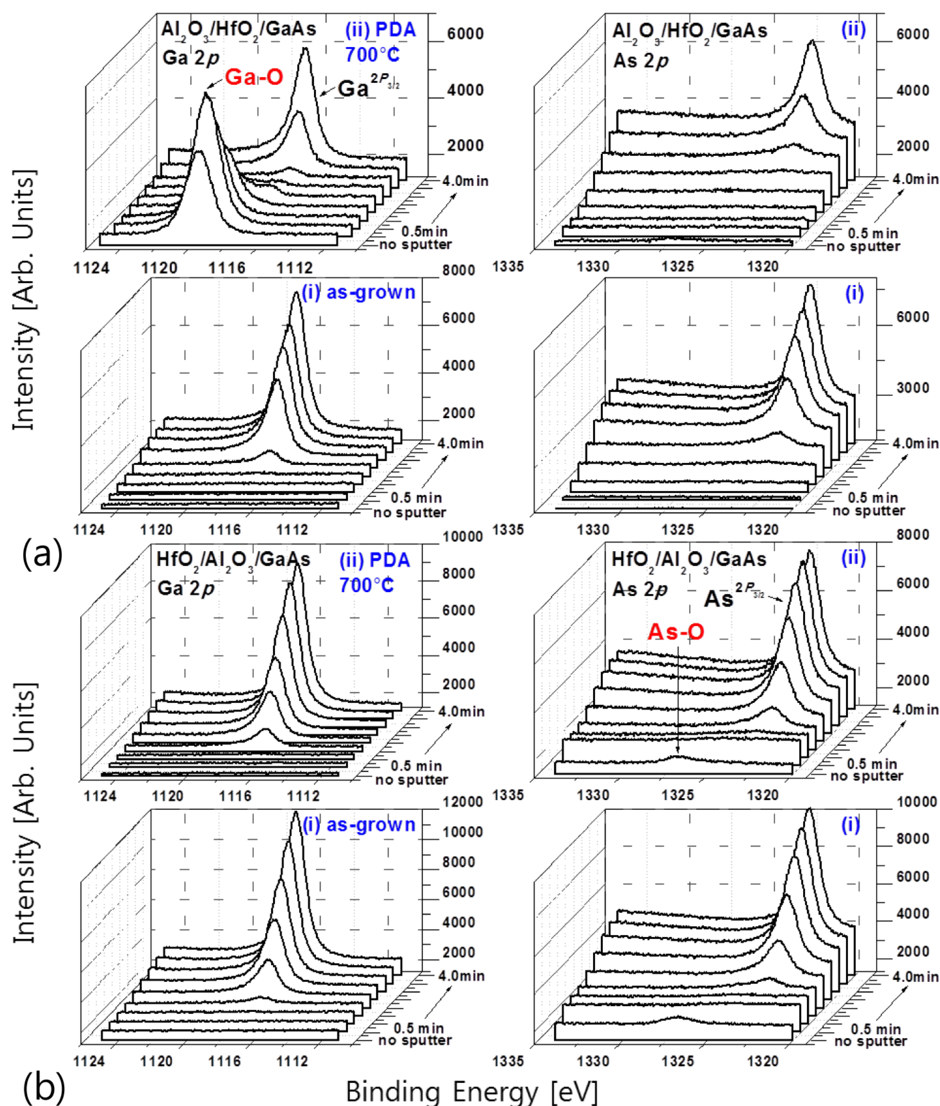

Figure 4. Ga 2p and As 2p core-level spectra of (a) Al_2O_3/HfO_2/GaAs and (b) HfO_2/Al_2O_3/GaAs samples as a function of Ne sputtering time.

elemental As at the HfO_2/GaAs interface was not detected after the PDA at 700 °C. Based on these results, we propose that both elemental Ga and As diffuse through the HfO_2 film during the PDA process. In particular, As atoms are easily converted to a higher oxidation state due to a thermally stable phase with a high negative Gibbs formation energy (−654.82 J/kmole for As_2O_3 and −927.04 J/kmole for As_2O_5) in a gaseous state over 278 °C. This permits it to diffuse out through the HfO_2 more easily than elemental Ga.

To confirm the formation of Ga and As oxides in the direction of the film depth, we applied XPS with Ne sputtering, as shown in Figure 4. Ga−O bonds in the annealed AH/GaAs at 700 °C increased after sputtering for 0.5 min but decreased with increased sputtering time (Figure 4a, left). These results indicate that the Ga−O bonds in AH/GaAs preferentially accumulate between the Al_2O_3 and HfO_2. Results from REELS measurements with a primary beam energy of 1000 eV support this conclusion through changes in the energy band gaps for the two samples (Table 1). The REELS results included

Table 1. Summary of Energy Band Gaps (E_g) for High-κ Oxide Films Grown on GaAs with Postannealing Temperature and Oxide Films[a]

samples	energy band gap values (eV)	
	as-deposited sample	PDA 700 °C
HfO_2/GaAs	5.51	4.72
Al_2O_3/GaAs	6.91	6.87
HfO_2/Al_2O_3/GaAs	5.55	5.54
Al_2O_3/HfO_2/GaAs	6.88	6.88

[a] E_g values were obtained by REELS with an electron beam energy at 1.0 keV. E_g values of Al_2O_3 and HfO_2 films are referenced to compare the effects of Ga−O.

information related to the energy loss of electrons that were reflected from the surface region to a thickness of 1.5−2 nm, which permitted band gaps (E_g) to be obtained for the surface layer. The formation of Ga oxides on the film surface would be reflected in the measured band gap. However, no changes in E_g were observed, although Ga and As oxides were clearly formed after the PDA. Therefore, we conclude that the out-diffusion of Ga was inhibited by the Al_2O_3 layer and that Ga oxides accumulated under the Al_2O_3 layer. In As 2p spectra, As−O states were observed faintly on the surface of the HfO_2 film in all samples, before and after the PDA. As discussed above, As oxides can readily transform to a gas phase below the film growth temperature. More As oxides were generated in the HA/GaAs structure because the Al_2O_3 layer was thinner than the AH/GaAs structure. Thus, although the As oxides diffused out during the annealing process, more As oxide states were trapped in the HA/GaAs surface layer during cooling after PDA than that for the AH/GaAs surface.

TEM measurements were carried out to investigate structural changes in the two oxides (Figure 5). The changes in the structural characteristics of the HfO_2 films in the two samples were clearly different after the PDA. The HfO_2 film annealed at 700 °C was fully crystallized, while no structural changes were observed in the case of the AH/GaAs samples. Considering the above findings on the effects of Ga oxide in HfO_2 films, we concluded that the formation of Ga oxides in HfO_2 had a significant suppressive effect on HfO_2 film crystallization. Therefore, the crystallization of HfO_2 on the Al_2O_3 layer resulted from the suppression in Ga oxide formation in the

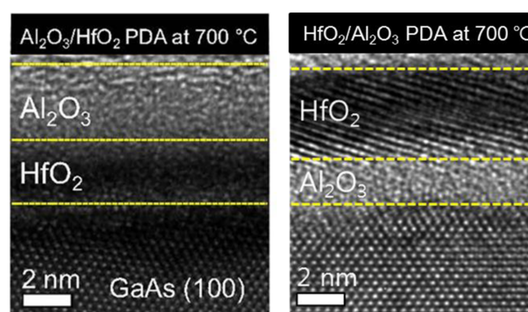

Figure 5. Cross-sectional HRTEM images of annealed Al_2O_3/HfO_2/GaAs and HfO_2/Al_2O_3/GaAs samples at 700 °C.

HfO_2 layer. We compared the thickness in the bottom oxides in the two types of samples, and found that the relative thicknesses of the bottom HfO_2 layers in annealed films were increased slightly, compared to the bottom Al_2O_3 layers. This indicated the incorporation of Ga oxides into the HfO_2. This result also supported the existence of a diffusion barrier of Al_2O_3 on GaAs.

Figure 6 shows a simplified reaction mechanism for the oxidation of Ga with the changes in diffusivity of the reactant

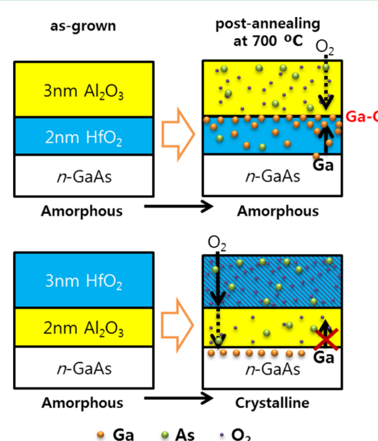

Figure 6. Schematic diagram of the interfacial reaction model for Al_2O_3/HfO_2/GaAs and HfO_2/Al_2O_3/GaAs samples after annealing at 700 °C.

O_2 and the decomposition of Ga and As from GaAs during annealing. We considered two possible reaction mechanisms. One was the formation of Ga and As oxides at the interface between high-κ oxide/GaAs followed by out-diffusion through the film. The other mechanism involved the out-diffusion of atomic Ga, followed by a reaction between the diffused atom and O_2. If the interfacial reaction between the reactant O_2 and substrate occurred at the GaAs surface, the oxidation caused by the interfacial reaction would depend only on the interdiffusion of external oxygen. Our experimental results indicated that more Ga−O bonds were generated in the AH/GaAs sample with a relatively thick Al_2O_3 layer. The main factor in the greater formation of Ga oxides with AH/GaAs was the out-diffusion of atomic Ga, because the Al_2O_3 layer blocked the out-diffusion of atomic Ga more effectively than the HfO_2 layer. The difference in oxygen diffusion was not found to be dependent on the thickness of Al_2O_3 and HfO_2. i.e., the oxygen for reaction with GaAs does not need to diffuse through the entire layer of Al_2O_3 and HfO_2. For the case of AH/GaAs after

a PDA at 700 °C, out-diffused Ga accumulated at the Al_2O_3/HfO_2 interface. Finally, an active reaction between interdiffused oxygen and accumulated Ga occurred at the Al_2O_3/HfO_2 interface. However, with HA/GaAs, the reaction between oxygen and the substrate was suppressed by Al_2O_3, which functioned a as a blocking layer and the diffusion of Ga through the Al_2O_3 layer was blocked because of the relatively low diffusivity of Ga in the Al_2O_3 layer. In summary, in both samples, the formation of interfacial oxides mainly appeared to be dependent on the oxygen diffusivity of the film. However, during annealing at temperatures higher than the decomposition temperature of Ga−As, the interfacial reaction was critically dependent on the difference in atomic Ga diffusivity between Al_2O_3 and HfO_2.

Electrical measurements using conductance and $C-V$ were carried out to investigate the dielectric characteristics of HA/GaAs and AH/GaAs. Figure 7a shows high-frequency $C-V$ curves for n-type GaAs measured at room temperature as a function of frequency (100 kHz, 500 kHz, and 1 MHz). We were not able to determine the true oxide capacitance of AH/GaAs and HA/GaAs because of the large frequency dispersion. However, we noted a large frequency dispersion in accumulation and depletion and the hysteresis loop both increased in AH/GaAs after PDA 700 °C compared to HA/GaAs. Previous reports have also reported a large frequency dispersion in conductance and $C-V$ measurements for high-κ dielectrics/III−V compound semiconductor systems. These reports verified that the high frequency dispersion was affected by the high interfacial states.[18−20] The C−V data reported herein indicate that the interface trap charge state in AH/GaAs with a PDA at 700 °C could be generated by the out-diffusion of atomic Ga. Thus, the Al_2O_3 buffer layer in HA/GaAs suppressed the generation of the interface trap state. When the two samples were compared, the difference in C−V curves was consistent with the conductance results shown in Figure 7(b) for the interfacial defect states of AH/GaAs and HA/GaAs before and after annealing. An important finding was that a defect state of ∼0.3 eV below the conduction band edge of GaAs increased strongly from 3.35×10^{13} to 1.65×10^{14} eV^{-1} cm^{-2} in AH/GaAs after a PDA at 700 °C. However, the defect state of HA/GaAs with a Al_2O_3 blocking layer remained unchanged. With the XPS data on depth profiles, these results suggest that the diffusion of Ga into the HfO_2 film led to the generation of a gap state in GaAs.

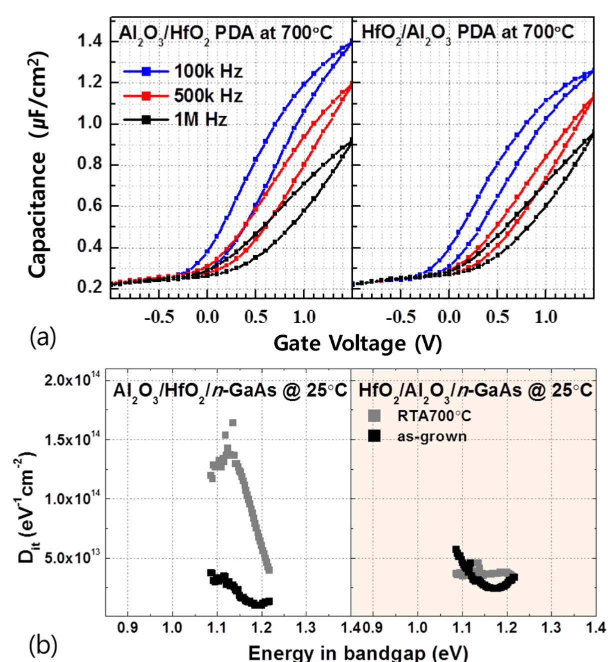

Figure 7. (a) $C-V$ curves of MOS structure with the TiN top electrode at several frequencies after an annealing treatment. (b) Conductance results before and after annealing for Al_2O_3/HfO_2/GaAs and HfO_2/Al_2O_3/GaAs samples at 25 °C.

DFT calculations were performed to verify the effects of Ga and As impurities in HfO_2. Panels a and b in Figure 8 provide information on the formation energies for various charged states of interstitial Ga (Ga_i) or interstitial As (As_i) inside m-HfO_2 or Al_2O_3 films, as a function of Fermi level with respect to the valence band maximum of a perfect sample of HfO_2. The band alignments for the HfO_2 film or the Al_2O_3 film on GaAs were assumed from XPS and REELS measurements (Figure 8a, b). Of note, the energy of formation of interstitial Ga inside the Al_2O_3 film was higher than that for the HfO_2 film. The values for the energy of formation for the interstitial Ga states in HfO_2 were negative within the band gap of GaAs, while the values for the energy of formation for the interstitial Ga states in Al_2O_3 were positive. This result indicated that interstitial Ga could not be generated in the Al_2O_3 film because of the unstable energy of formation. The above findings provide support for our conclusion that the Al_2O_3 layer suppressed the diffusion of atomic Ga. The diffusion of Ga and the formation of gap states in GaAs were directly correlated. Considering the lowest energy of formation in the band gap of GaAs, As_i^{+2}, Ga_i^{+}, the Ga_i^{-} charged states were energetically more stable than the Ga_i state. Thus, we conclude that Ga and As interstitials are the origins of the defect state within the HfO_2 band gap. Total density of states for m-HfO_2, interstitial As_i^{+2}, Ga_i^{+}, and Ga_i^{-} in m-HfO_2 was calculated (Figure 8c). The arrows indicate the Fermi energy level. In the total DOS results for perfect m-HfO_2, the occupied states below the Fermi level were composed of bands that were mainly composed of O 2p states and Hf 5d states, as the result of covalent bonding between Hf and O atoms. The unoccupied states were induced from spin−orbit coupling between the O 2p orbitals and electrons of Hf 5d and 6s. New peaks were observed in interstitial As_i^{+2}, Ga_i^{+}, and Ga_i^{-} in m-HfO_2. These changes could be induced by local symmetry distortions or changes in the local coordination of Ga or As interstitials. Interstitial Ga incorporated into m-HfO_2 induced defect states in the band gap of HfO_2, which originated mainly from the s-orbital of Ga for lower energy states and the p-orbitals of Ga for higher energy states. The defect states for interstitial As incorporating m-HfO_2 were derived from the p-orbital of As. However, the energy levels of the unoccupied defect states for interstitial As in the band gap of HfO_2 could be shifted by a correction involving a scissoring operation. For the band gap of HfO_2 measured by REELS, a scissoring operation was used to correct the estimates of the band gap because the excitation state to the energy level of the unoccupied states could not be precisely predicted by DFT calculation. The energy levels containing defect states are represented in Figure 8d as a function of the charging state of interstitial Ga in HfO_2. The gap state within the band gap of GaAs was induced by interstitial Ga in the m-HfO_2. We propose that the energy level of the gap states, which are indicated by arrows, corresponds to the defect level at ∼0.3 eV below the conduction band edge of GaAs in our previous conductance results.

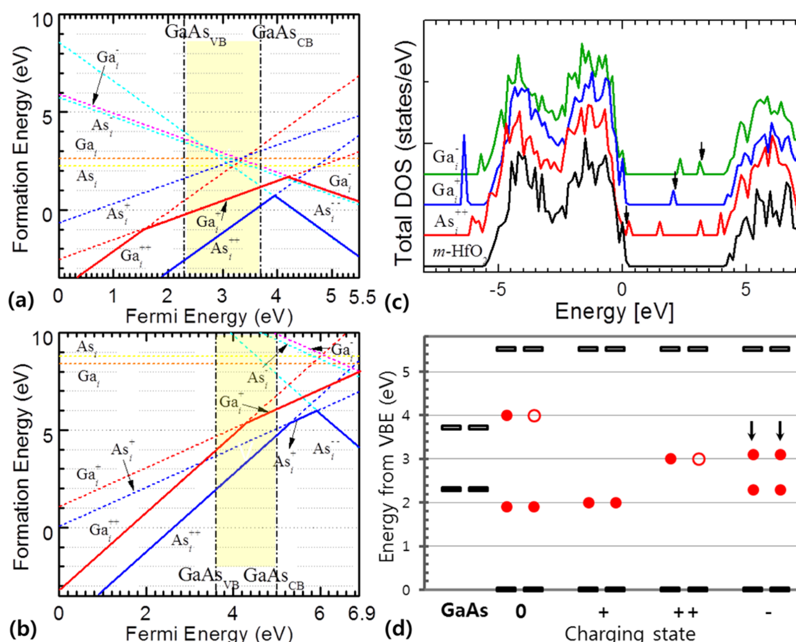

Figure 8. Defect formation energies of Ga or As impurities in HfO_2 or Al_2O_3. (a) Formation energy versus Fermi level for Ga or As interstitial in HfO_2 and (b) for Ga or As interstitial in Al_2O_3. Band alignments were by XPS and REELS measurements. Yellow, band gap of GaAs. (c) Total density of states for Ga- and As- related defects in HfO_2. (d) Energy band diagram of defect states for *m*-HfO_2/GaAs. Filled circle, occupied state; open circle, unoccupied state.

4. CONCLUSION

In summary, we investigated bilayer stacked high-κ oxide dielectrics consisting of HfO_2/Al_2O_3 films and Al_2O_3/HfO_2 films grown on *n*-GaAs (100) using atomic layer deposition. Our goal was to interpret the interfacial states and to examine the impact of postannealing treatment. XPS data for as-grown sample indicated that controlling the thickness of the Al_2O_3 layer in the stack structure on GaAs could cause a substantial reduction in native oxide formation. After an annealing treatment at 700 °C, Ga−O bond formation increased substantially in AH/GaAs compared with HA/GaAs. Moreover, a higher D_{it} and larger frequency dispersion were observed in AH/GaAs after a PDA at 700 °C. Investigations of the films indicated that (1) the Al_2O_3 layer effectively suppressed the diffusion of external oxygen as compared to that of HfO_2; (2) the Al_2O_3 layer blocked the diffusion of atomic Ga more effectively than HfO_2; (3) the stacked HfO_2−Al_2O_3 film with a Al_2O_3 buffer layer in contact with GaAs suppressed the generation of interfacial defect states in the band gap of GaAs by blocking the diffusion of Ga into the HfO_2 film. The findings indicate that device performances can be improved when a Al_2O_3 passivation layer is applied to HfO_2/GaAs structure. The equivalent oxide thickness (EOT) in HfO_2/GaAs can be decreased by the controlling the thickness of the Al_2O_3 passivation layer. It should be noted that, the use of a Al_2O_3 buffer layer in contact with the GaAs substrate can aid in improving electrical properties such as mobility and threshold voltage shift on thermal stability. From our conductance results, we expected that Ga would easily out-diffuse into HfO_2 during an annealing at 700 °C, which would induce a high D_{it}, resulting in a degradation in carrier mobility due to an increase in Coulomb scattering. Moreover, interstitial Ga^- charged states in HfO_2 during annealing at 700 °C can induce threshold voltage shifts. Therefore, we conclude that electrical properties in the case of thermal stability are enhanced by the presence of a Al_2O_3 blocking layer.

AUTHOR INFORMATION

Corresponding Author

*E-mail: mh.cho@yonsei.ac.kr.

Present Address

‡C.Y.K. is currently at Department of Material Characterization, LG R&D Campus, 137-724, Korea

Notes

The authors declare no competing financial interest.

ACKNOWLEDGMENTS

This work was partially supported by an Industry-Academy joint research program between Samsung Electronics-Yonsei University and a grant of the "Next-generation substrate technology for high performance semiconductor devices (KI002083)" from the Ministry of Knowledge Economy of Korea.

REFERENCES

(1) Seguini, G.; Perego, M.; Spiga, S.; Fanciulli, M. *Appl. Phys. Lett.* **2007**, *91*, 192902.

(2) Hackley, J. C.; Demaree, J. D.; Gougousi, T. *Appl. Phys. Lett.* **2008**, *92*, 162902.

(3) Lin, H. C.; Yang, Y.; Sharifi, H.; Kim, S. K.; Xuan, Y.; Shen, T.; Mohammadi, S.; Ye, P. D. *Appl. Phys. Lett.* **2007**, *91*, 212101.

(4) Shahrjerdi, D.; Akyol, T.; Ramon, M.; Garcia-Gutierrez, D. I.; Tutuc, E.; Banerjee, S. K. *Appl. Phys. Lett.* **2008**, *92*, 203505.

(5) Hinkle, C. L.; Sonnet, A. M.; Vogel, E. M.; McDonnell, S.; Hughes, G. J.; Milojevic, M.; Lee, B.; Aguirre-Tostado, F. S.; Choi, K. J.; Kim, H. C.; Kim, J.; Wallace, R. M. *Appl. Phys. Lett.* **2008**, *92*, 071901.

(6) Chang, C.-H.; Chiou, Y.-K.; Chang, Y.-C.; Lee, K.-Y.; Lin, T.-D.; Wu, T.-B.; Hong, M. *Appl. Phys. Lett.* **2006**, *89*, 242911.

(7) Kim, C. Y.; Cho, S. W.; Cho, M.-H.; Chung, K. B.; An, C.-H.; Kim, H.; Lee, H. J.; Ko, D.-H. *Appl. Phys. Lett.* **2008**, *93*, 192902.
(8) Suh, D. Ch.; Cho, Y. D.; Kim, S. W.; Ko, D.-H.; Lee, Y.; Cho, M.-H.; Oh, J. *Appl. Phys. Lett.* **2010**, *96*, 142112.
(9) Cho, M.-H.; Chang, H. S.; Moon, D. W.; Kang, S. K.; Min, B. K.; Ko, D.-H.; Kim, H. S.; McIntyre, P. C. *Appl. Phys. Lett.* **2004**, *84*, 1171−1173.
(10) Zhao, H.; Huang, J.; Chen, Y.-T.; Yum, J. H.; Wang, Y.; Zhou, F.; Xue, F.; Lee, J. C. *Appl. Phys. Lett.* **2009**, *95*, 253501.
(11) Contreras-Guerrero, M., R.; Lopez-Lopez, M.; Kim, J.; Wallace, R. M. *Appl. Phys. Lett.* **2009**, *95*, 212902.
(12) Zhang, S. B.; Northrup, J. E. *Phys. Rev. Lett.* **1991**, *67*, 2339−2342.
(13) Chang, C.-H.; Chiou, Y.-K.; Chang, Y.-C.; Lee, K.-Y.; Lin, T.-D.; Wu, T.-B.; Hong, M.; Kwo, J. *Appl. Phys. Lett.* **2006**, *89*, 242911.
(14) Hollinger, G.; Skheyta-Kabbani, R.; Gendry, M. *Phys. Rev. B* **1994**, *49*, 11159−11167.
(15) Suri, R.; Lichtenwalner, D. J.; Misra, V. *Appl. Phys. Lett.* **2010**, *96*, 112905.
(16) McDonnell, S.; Dong, H.; Hawkins, J. M.; Brennan, B.; Milojevic, M.; Aguirre-Tostado, F. S.; Zhernokletov, D. M.; Hinkle, C. L.; Kim, J.; Wallace, R. M. *Appl. Phys. Lett.* **2012**, *100*, 141606.
(17) F, T. E.; Chu, W. K.; Aselage, T. L.; Picraux, S. T. *Appl. Phys. Lett.* **1986**, *49*, 666.
(18) Hwang, Y.; Engel-Herbert, R.; Rudawski, N. G.; Stemmer, S. *Appl. Phys. Lett.* **2010**, *96*, 102910.
(19) Martens, K.; Wang, W. F.; Dimoulas, A.; Borghs, G.; Meuris, M.; Groeseneken, G.; Maes, H. E. *Solid-State Electron.* **2007**, *51*, 1101−1108.
(20) Ok, I.; Kim, H.-s.; Zhang, M.; Kang, C.-Y.; Rhee, S. J.; Choi, C.; Krishnan, S. A.; Lee, T.; Zhu, Feng; Gaurav, T.; Lee, J. C. *IEEE Electron Device Lett.* **2006**, *27*, 145−147.